Provided for non-commercial research and education use.
Not for reproduction, distribution or commercial use.

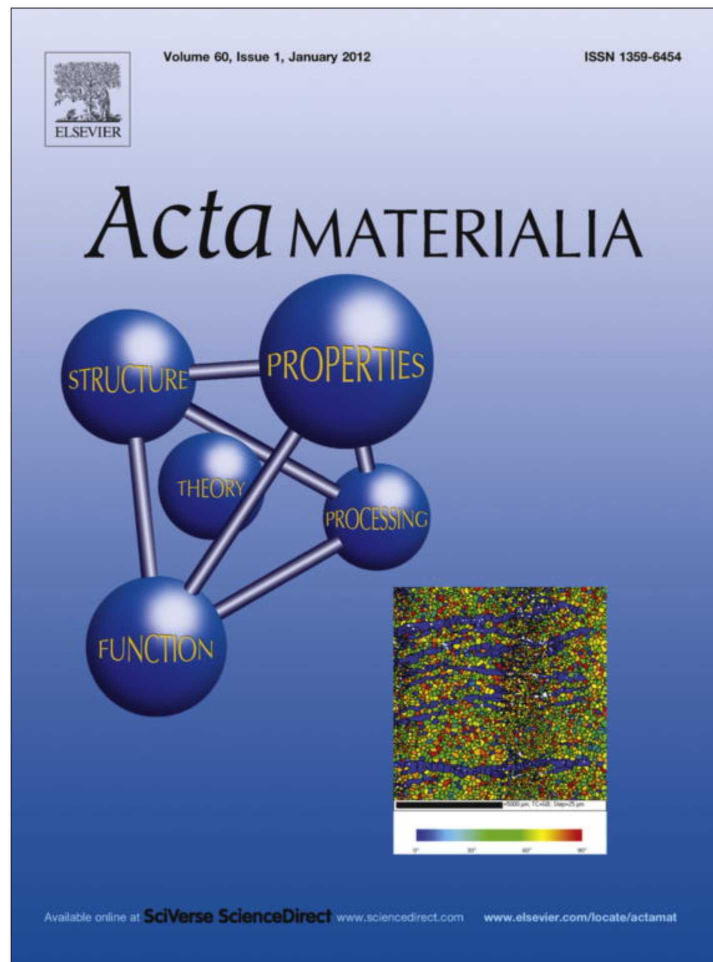

(This is a sample cover image for this issue. The actual cover is not yet available at this time.)

This article appeared in a journal published by Elsevier. The attached copy is furnished to the author for internal non-commercial research and education use, including for instruction at the authors institution and sharing with colleagues.

Other uses, including reproduction and distribution, or selling or licensing copies, or posting to personal, institutional or third party websites are prohibited.

In most cases authors are permitted to post their version of the article (e.g. in Word or Tex form) to their personal website or institutional repository. Authors requiring further information regarding Elsevier's archiving and manuscript policies are encouraged to visit:

http://www.elsevier.com/copyright

Author's personal copy

Available online at www.sciencedirect.com

SciVerse ScienceDirect

Acta Materialia 60 (2012) 3296–3301

www.elsevier.com/locate/actamat

Phase-field simulations of thickness-dependent domain stability in $PbTiO_3$ thin films

G. Sheng [a,*], J.M. Hu [b], J.X. Zhang [c], Y.L. Li [d], Z.K. Liu [a], L.Q. Chen [a]

[a] Department of Materials Science and Engineering, The Pennsylvania State University, University Park, PA 16802, USA
[b] Department of Materials Science and Engineering, Tsinghua University, Beijing 100084, People's Republic of China
[c] GE Aviation, 111 Merchant Street, Cincinnati, OH 45246, USA
[d] Pacific Northwest National Laboratory, Richland, WA 99352, USA

Received 6 August 2011; received in revised form 12 January 2012; accepted 2 March 2012

Abstract

The phase-field approach is used to predict the effect of thickness on domain stability in ferroelectric thin films. The mechanism of strain relaxation and the critical thickness for dislocation formation from both the Matthews–Blakeslee and People–Bean models are employed. Thickness–strain domain stability diagrams are obtained for $PbTiO_3$ thin films for different strain relaxation models. The relative domain fractions as a function of film thickness are also calculated and compared with experimental measurements in $PbTiO_3$ thin films grown on $SrTiO_3$ and $KTaO_3$ substrates.
© 2012 Acta Materialia Inc. Published by Elsevier Ltd. All rights reserved.

Keywords: Phase-field models; Ferroelectricity; Thin films; Simulation

1. Introduction

It is well established that the domain/phase stabilities in epitaxial ferroelectric thin films are controlled by both the mechanical and electrical boundary conditions [1,2]. It is also known that the misfit strain will have a significant impact on the Curie transition temperature [3,4]. With an increasing demand for portability of electronics devices it is crucial to understand the effect of size on the properties of active components in these devices. For example, for ferroelectric thin films it has long been believed that there is a critical size below which spontaneous polarization cannot be sustained [5,6]. Fong et al. [7] reported the relationship between the ferroelectric transition temperature T_c and film thickness, providing experimental evidence of ferroelectricity in ultra-thin $PbTiO_3$ films down to a thickness of 12 Å, corresponding to three unit cells. In earlier reports the critical thickness for ferroelectricity in $BaTiO_3$ film [8] was predicted to be of the order of 10–15 nm at room temperature, and for PZT ferroelectricity was observed in films [9] as thin as 4 nm. The thickness-dependent evolution of ferroelectric phases and related domain structures under different mechanical and electric boundary conditions have been reported for a series of thin film systems [4–13].

In earlier theoretical models on misfit strain–temperature diagrams, including thermodynamic calculations [14,15] and ab initio methods [16,17], as well as phase-field simulations [18,19], the boundary and geometric or size conditions are treated as independent parameters. Thickness-dependent effects like strain relaxation were not included. In all these models the ferroelectric film is assumed to be fully constrained by the underlying substrate, which will generate internal stresses. The ferroelectric transition below the Curie temperature will induce eigenstrain in the film. When the internal stresses due to lattice misfit are too large this assumption is inappropriate, because the stresses would be immediately relaxed. There are generally two means of stress relaxation: formation of a periodic pattern of interfacial

* Corresponding author. Present address: Scientific Forming Technologies Corporation, Columbus, OH 43235, USA.
E-mail address: shengguang1982@gmail.com (G. Sheng).

1359-6454/$36.00 © 2012 Acta Materialia Inc. Published by Elsevier Ltd. All rights reserved.
http://dx.doi.org/10.1016/j.actamat.2012.03.003

Author's personal copy

dislocations at the film–substrate interface at the growth temperature and ferroelastic twin formation below the Curie temperature. Thus the effect of misfit strain on the domain stability may be heavily overestimated and needs to be reinvestigated.

Modeling thickness-dependent domain stability in ferroelectrics was pioneered by Roytburd et al. [20] using thermodynamic analysis of polydomain heterostructures, using an effective substrate lattice parameter as a function of dislocation density, which depends on the critical film thickness for dislocation generation. The predicted *c* domain fractions as a function of film thickness showed very good agreement with the experimental values in (001) $PbTiO_3$ thin films grown on MgO and $SrTiO_3$ substrates. Roytburd et al. [21] also presented a detailed thermodynamic analysis and phase-field simulations for the cubic–tetragonal transformation in a constrained ferroelectric layer, and generated a thickness–strain domain stability diagram for a $PbTiO_3$–$ZrTiO_3$ system (Pb > 60%). Recently Qiu et al. employed a similar non-linear Landau–Ginzburg–Devonshire thermodynamic model to construct thickness–strain domain stability diagrams for (001) oriented $PbTiO_3$ [22] and $PbZr_{1-x}Ti_xO_3$ (PZT) [23] epitaxial thin films. They compared the critical thickness of dislocation formation estimated using the classical Matthews–Blakeslee (MB) [24,25] and People–Bean (PB) model [26,27], demonstrating that thickness-dependent properties like effective strain and phase stabilities could be very different depending on the model used [22,23]. A similar approach was applied to $Ba_{0.5}Sr_{0.5}TiO_3$ and $SrTiO_3$ thin films [28], and the corresponding thickness-dependent properties were calculated.

In this paper we will extend the previous phase-field model [18,19] to study thickness-dependent domain stabilities by including strain relaxation mechanisms to calculate the real effective strain as a function of film thickness. Using a $PbTiO_3$ thin film as a representative example we will compare thickness–strain domain stability diagrams constructed using both the MB and PB (PB) models. We will also report the domain fractions as a function of film thickness in $PbTiO_3$ thin films grown on $SrTiO_3$ and $KTaO_3$ substrates, and compare the simulation results with experimental measurements.

2. Theory

In this work the thickness-dependent properties of strained ferroelectric films are modeled using the segregation model [28]. In this model all the misfit dislocations are assumed to reside only within a thin buffer layer with thickness h_B, which is much smaller than the film thickness h. This assumption is different from other approaches where the dislocations are assumed to be uniformly distributed within the whole film [29]. When the film thickness exceeds the critical thickness limit for dislocation formation elastic relaxation will occur but the strain in the film will still be homogeneous. The pseudomorphic misfit strain, here referred to as the "ideal misfit strain", is calculated as $\varepsilon_0 = (a_s - a_f)/a_f$, where a_s and a_f are the substrate and film lattice parameters, respectively, at room temperature. The actual misfit strain or effective misfit strain $\varepsilon(h)$ at room temperature as a function of thickness is estimated as [22]:

$$\varepsilon(h) = 1 - \frac{(1-\varepsilon_0)}{1-\varepsilon_0(1-h_c/h)} \quad (1)$$

where h_c is the critical thickness for dislocation formation.

For ferroelectric films Speck and Pompe [24] applied the MB model [25] to calculate the critical thickness for dislocation formation. However, the MB model was originally developed for metals and it has been shown that the critical thickness in semiconductor films will be strongly underestimated using this model, especially at relatively low strains [26,27,30–32]. In ferroelectric thin films, the critical thickness is also underestimated by MB model. For example, for a $PbTiO_3$ thin film grown on a (001) $SrTiO_3$ substrate the critical thickness predicted by the MB model is only 6.2 nm [33]. The MB model is also not applicable to high quality films and substrates, since initial dislocations are absent in these systems and there will be a significant energy barrier for nucleation of dislocations during the growing process [26,27,30–32]. Alternative models were developed by People and Bean [26,27], which explains the observed critical thickness for semiconductor films much better than the MB model [26,27,30]. Thus in this paper we will employ both the MB and PB models to determine the critical thickness for dislocation formation and compare the simulation results from the two models.

The critical thickness for dislocation formation has been given by Speck and Pompe [24] for the MB model and by Marée et al. [30] for the PB model:

$$h_c^{MB} = \frac{\bar{b}(1-\nu\cos^2\beta)}{8\pi\cos\lambda(1+\nu)}\frac{1}{\varepsilon_0}\ln\left(\alpha\frac{h_c^{MB}}{\bar{b}}\right) \quad (2)$$

$$h_c^{PB} = \frac{\bar{b}(1-\nu)}{40\pi(1+\nu)}\frac{1}{\varepsilon_0^2}\ln\left(\frac{h_c^{PB}}{\bar{b}}\right) \quad (3)$$

where ε_0 is the ideal misfit strain, $\bar{b}$ is the magnitude of the Burgers vector, ν is the Poisson ratio, α is the cut-off parameter describing the sub-continuum energy of the dislocation core, β is the angle between the dislocation line and the Burgers vector, and λ is the angle between the Burgers vector and a line that lies within the interface and in a plane normal to the dislocation line. For the cubic on cubic epitaxy of perovoskites like $PbTiO_3$ the misfit dislocations will have a $\langle 110 \rangle$ type Burgers vector, pure edge character ($\beta = 90°$) and a 45° inclined to the film/substrate interface $\lambda = 45°$) [24]. The cut-off parameter $\alpha = 4$ and the Poisson ratio is 0.33 [22,33].

The critical thickness for dislocation formation predicted by the MB and PB models are plotted in Fig. 1 as a function of the ideal misfit strain. The *x*-axis in Fig. 1 only includes the tensile strain, since the critical thickness is independent of the sign of the strain, i.e. the same magnitude of tensile and compressive strain will result in the same critical thickness. It is shown that for the same ideal

Author's personal copy

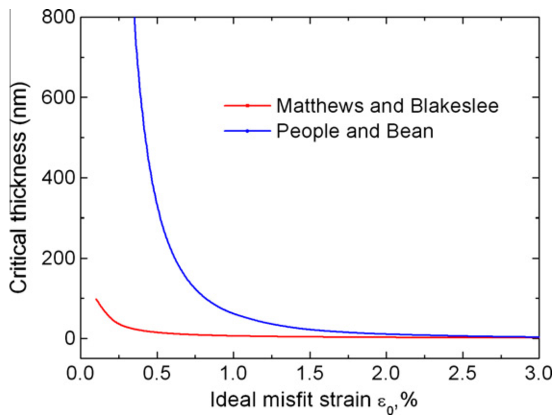

Fig. 1. Theoretical MB and PB critical thickness values for misfit dislocation formation in $PbTiO_3$ thin films as a function of misfit strain at room temperature $T = 25$ °C.

misfit strain the PB model will give a much larger critical thickness than the MB model when the ideal misfit strain is less than 2.0%. For example, for cubic $PbTiO_3$ on $SrTiO_3$ at room temperature the critical thicknesses according to the MB and PB models are 6.2 [33] and 48 nm, respectively, corresponding to an ideal misfit strain ε_0 of about 1.28% of the compressive strain. The calculated MB critical thickness in Fig. 1 is essentially the same as that presented in Qiu et al. [22].

The actual or real misfit strain can be calculated as a function of thickness based on the critical thickness determined from either the MB or PB model using Eq. (1), and two examples are given in Figs. 2 and 3 for $PbTiO_3$ thin films grown on $SrTiO_3$ and $KTaO_3$ substrates, respectively. As mentioned above, the ideal misfit strain ε_0 for cubic $PbTiO_3$ on cubic $SrTiO_3$ at room temperature is estimated to be −1.28%, from the lattice parameter mismatch of cubic unstrained $PbTiO_3$ (3.956 Å [33]) and $SrTiO_3$ (3.905 Å [34]). Similarly, the misfit strain for a $PbTiO_3$ thin film on a $KTaO_3$ substrate is about 0.83% of the tensile strain, from the lattice parameters of cubic $PbTiO_3$ and

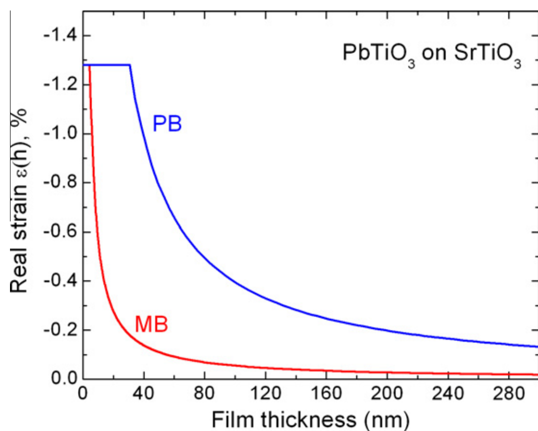

Fig. 2. Calculated actual misfit strains as a function of thickness using both the MB and PB models for $PbTiO_3$ thin films grown on $SrTiO_3$ substrates at $T = 25$ °C.

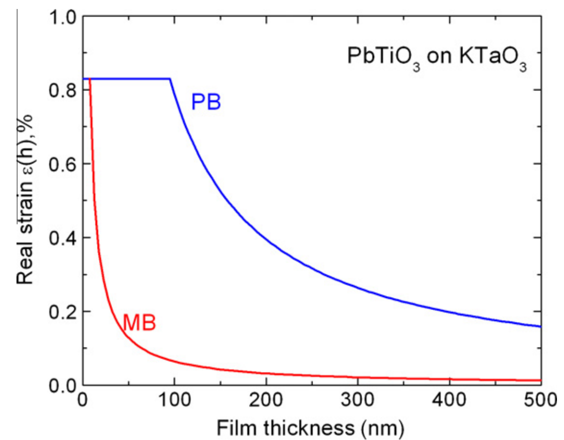

Fig. 3. Calculated actual misfit strains as a function of thickness using both the MB and PB models for $PbTiO_3$ thin films grown on $KTaO_3$ substrates at $T = 25$ °C.

$KTaO_3$ (3.989 Å [34,35]), also at room temperature. Here the estimated strain values using the room temperature lattice constants are different from those calculated with the growth temperature lattice constants for $PbTiO_3$, $SrTiO_3$ and $KTaO_3$ [22], but should still be a reasonable estimation of the room temperature strain states in these two systems.

In the phase-field model of ferroelectric thin films the spontaneous polarization vector $P(x) = (P_1,\ P_2,\ P_3)$ is chosen as the order parameter and its spatial and temporal evolutions are governed by the time-dependent Ginzburg–Landau equations:

$$\frac{\partial P_i(x,t)}{\partial t} = -L\frac{\delta F}{\delta P_i(x,t)}, \quad i = 1,2,3, \tag{4}$$

where L is the kinetic coefficient related to domain wall mobility and F is the total free energy of the system. $\delta F/\delta P_i(x,t)$ is the thermodynamic driving force for the spatial and temporal evolution of $P_i(x,t)$. The total free energy F includes the bulk free energy, elastic deformation energy, domain wall energy and electrostatic energy, i.e.

$$F = \int_V [f_{bulk}(P_i) + f_{elas}(P_i,\varepsilon_{ij}) + f_{wall}(P_{i,j}) + f_{elec}(P_i,E_i)]dV \tag{5}$$

where V is the volume of the film and $dV = dx_1dx_2dx_3$. The bulk free energy density of $PbTiO_3$ is described by a six order Landau–Devonshire polynomial [36] with free energy coefficients taken from the literature [14,37]: $\alpha_1 = 3.8(T-479)\times10^5$; $\alpha_{11} = -7.3\times10^7$; $\alpha_{12} = 7.5\times10^8$; $\alpha_{111} = 2.6\times10^8$; $\alpha_{112} = 6.1\times10^8$; $\alpha_{123} = -3.7\times10^9$; $c_{11} = 1.746\times10^{11}$; $c_{12} = 7.937\times10^{10}$; $c_{44} = 1.11\times10^{11}$; $Q_{11} = 0.089$; $Q_{12} = -0.026$; $Q_{44} = 0.0675$ (in SI units and T in °C). A description of the domain wall energy and electrostatic energy can be found in our previous publications [18,19,38].

The elastic energy density is given by:

$$f_{elas} = \frac{1}{2}c_{ijkl}e_{ij}e_{kl} = \frac{1}{2}c_{ijkl}(\varepsilon_{ij}-\varepsilon^0_{ij})(\varepsilon_{kl}-\varepsilon^0_{kl}) \tag{6}$$

Author's personal copy

where $e_{ij} = \varepsilon_{ij} - \varepsilon^0_{ij}$ is the elastic strain, ε_{ij} is the total strain of the film compared with the parent paraelectric phase, and c_{ijkl} is the elastic stiffness tensor. Both ε_{ij} and ε^0_{ij} are defined using the cubic phase as the reference, and $\varepsilon^0_{ij} = Q_{ijkl}P_kP_l$, where Q_{ijkl} is the electrostrictive coefficient tensor. The details of the calculation of the total strain ε_{ij} in a (001)-oriented film under a biaxial strain are described in our previous publications [18,19]. In this work the average film/substrate misfit strains $\bar{\varepsilon}_{11} = \bar{\varepsilon}_{22} = \varepsilon(h)$ along the x- and y-axes, and $\varepsilon(h)$ is dependent on the film thickness and is given by Eq. (1). Here we assume $\bar{\varepsilon}_{12} = \bar{\varepsilon}_{21} = 0$. The overbar indicates an average over the film.

A rectangular coordinate system, $x = (x_1, x_2, x_3)$ is set up with the x_1-, x_2-, and x_3-axes along the [100], [010], and [001] crystallographic directions, respectively. We employed a $128\Delta x$ grid size along the x_1- and x_2-axes, with periodic boundary conditions. $\Delta x = 1$ nm is the spacing between the two nearest grid points. We vary the thickness of the film from several to hundreds of nanometers. The actual strain is calculated using Eq. (1) if the thickness exceeds the critical thickness determined from the MB (Eq. (2)) or PB (Eq. (3)) models. The short-circuit electric boundary condition is employed to compute the dipole–dipole interactions [38].

3. Results and discussions

3.1. Thickness–strain domain stability diagrams

To construct the thickness–strain domain stability diagram for $PbTiO_3$ thin films we performed a series of simulations under different strains and thicknesses to obtain the corresponding domain stabilities. Here we present three types of phase diagrams with different strain relaxation mechanisms: Fig. 4 is the thickness–strain domain stability diagram without considering strain relaxation, while Figs. 5 and 6 are the domain stability diagrams using the MB and PB models to evaluate the actual misfit strains as a function of film thickness, respectively.

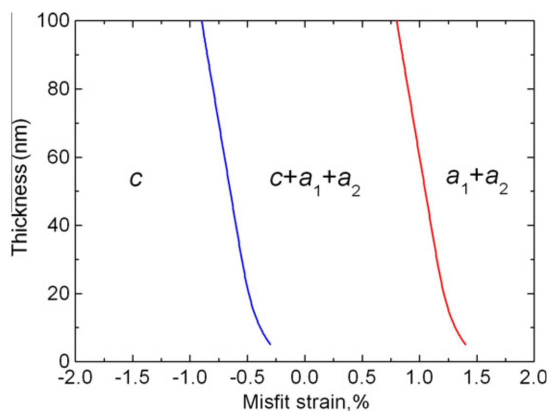

Fig. 4. Thickness–strain domain stability diagram of $PbTiO_3$ thin films at $T = 25$ °C, without considering strain relaxation as a function of film thickness.

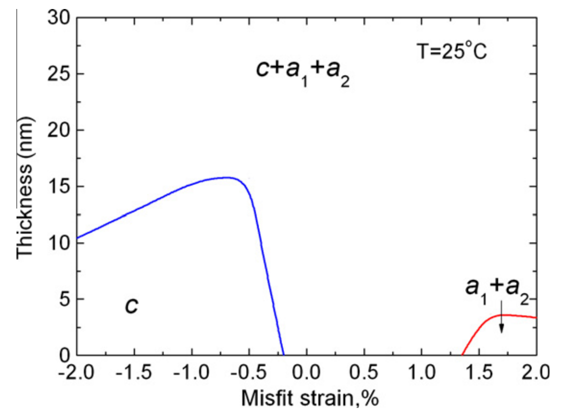

Fig. 5. Thickness–strain domain stability diagram of $PbTiO_3$ thin films at $T = 25$ °C, using the MB model for critical thickness estimation.

Since a uniform misfit strain without any thickness-dependent relaxation is assumed in Fig. 4 the only cause of the shift in phase boundaries as a function of thickness is the effect of electrostatic interactions. It can be observed that the boundary separating the c domain region and the $c + a_1 + a_2$ multi-domain region shifts to the left with increasing thickness, indicating shrinking of the c domain region in thicker films. This is because this simulation employs the short-circuit boundary condition which favors c domains. As the film becomes thicker the effect of the boundary condition becomes smaller and the fraction of c domains decreases slightly. A similar trend is observed in the tensile strain regions, where the $c + a_1 + a_2/a_1 + a_2$ phase boundaries also shift to the left, indicating that a thin film of small thickness will promote the formation of c domains.

The thickness–strain domain stability diagrams presented in Figs. 5 and 6, which include strain relaxation due to the increase in thickness, exhibit significant differences from Fig. 4. In both Figs. 5 and 6 the x-axis is the ideal strain due to the lattice mismatch, which could only be maintained below the critical thickness for dislocation formation. When the thickness of the film exceeds this critical value the real or actual strain is determined by Eqs. (2)

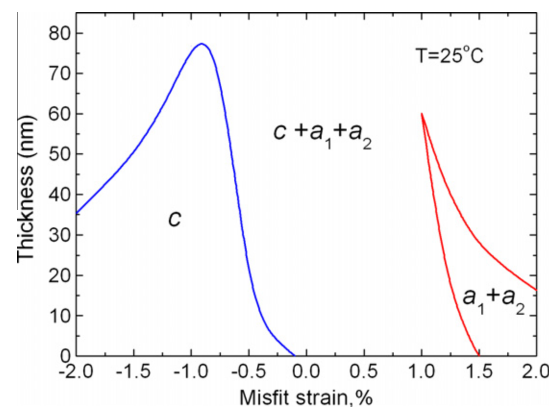

Fig. 6. Thickness–strain domain stability diagram of $PbTiO_3$ thin films, using the PB model for critical thickness estimation.

Author's personal copy

or (3), and the corresponding domain stabilities at this thickness can be found in Figs. 5 or 6, depending on whether the MB or PB criteria are used for the critical thickness calculation. The MB model predicts very limited strain regions for the formation of pure c or $a_1 + a_2$ domains, as shown in Fig. 5, indicating that all the $PbTiO_3$ films with a thickness of 20 nm or more will form the $c + a_1 + a_2$ multi-domain state. As discussed above, the PB model gives a much larger critical thickness for strain relaxation compared with the MB model, and results in a much wider region for pure c and $a_1 + a_2$ phases, as illustrated in Fig. 6.

3.2. Comparison with experiments

The relative domain fractions as a function of film thickness have been measured using various methods for $PbTiO_3$ thin films grown on different substrates. Kwak et al. [39] reported the c domain fraction as a function of film thickness over a wide thickness range from 30 to about 700 nm for $PbTiO_3$ thin films grown on (001) $KTaO_3$ substrates using metal organic chemical vapor deposition. Similarly, Hsu and Raj [40] grew $PbTiO_3$ thin films with thicknesses of from 50 to 350 nm on (001) $SrTiO_3$ substrates using pulsed laser ablation and measured the relative volume fraction of the $a_1 + a_2$ domains based on mapping of the X-ray diffraction intensity distribution in the reciprocal space. From phase-field simulations it is straightforward to count the populations or volume fractions of different domain variants from the simulated domain structures, which allows us to compare the simulation results with the experimental measurements in the two systems discussed above.

The calculated c domain fractions as a function of thickness in $PbTiO_3$ films on $KTaO_3$ are plotted in Fig. 7, using both the MB and PB models. Experimental data from Kwak et al. [39] are also included for comparison. The real misfit strain as a function of film thickness in this system is given in Fig. 3. It can be seen that both models predict increasing c domain fractions with increasing thickness,

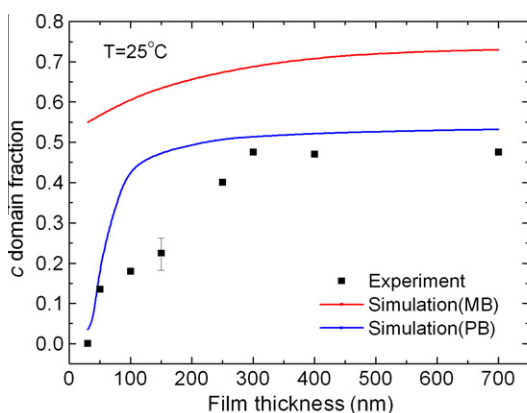

Fig. 7. Calculated and experimental c domain fractions [39] as a function of thickness in $PbTiO_3$ thin films grown on (001) $KTaO_3$ substrates.

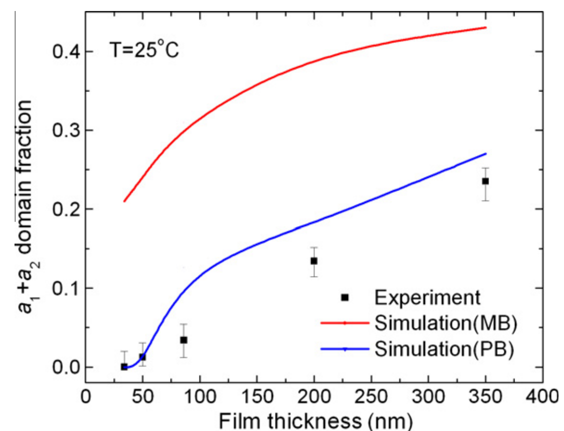

Fig. 8. Calculated and experimental $a_1 + a_2$ domain fractions [40] as a function of thickness in $PbTiO_3$ thin films grown on (001) $SrTiO_3$ substrates.

as observed experimentally. This is because a $PbTiO_3$ thin film grown on a $KTaO_3$ substrate is subjected to tensile strain. Increasing the film thickness will relax the tensile strain and promote the formation of c domains. It has also been demonstrated that the simulation results from the PB model quantitatively agree well with the experiment results, indicating a better estimation of the critical thickness for dislocation formation than the MB model, which gives a much higher c domain fraction, as shown in Fig. 7. This may imply that the MB model overestimates the relaxation of strain, especially for films with small thickness. Fig. 8 is a plot of the volume fraction of $a_1 + a_2$ domains in $PbTiO_3$ films on $SrTiO_3$ together with the experimental data [40]. In this case the $PbTiO_3$ thin film is compressively strained and increasing film thickness will produce more $a_1 + a_2$ domains. Again, the PB model demonstrates excellent agreement with the experimental data for this system.

4. Summary

In this paper we have used a three-dimensional phase-field model to predict the effect of thickness on domain stability in ferroelectric films. The model takes into account the ferroelectric domain structure and the electrostrictive effect, as well as strain relaxation due to the thickness effect. As an example, the thickness–strain domain stability diagram was constructed for $PbTiO_3$ thin films, using both the MB and PB models to estimate the critical thickness and strain relaxation. The relative domain populations as functions of thickness are plotted for $PbTiO_3$ thin films grown on $SrTiO_3$ and $KTaO_3$ substrates and compared with available experimental results. It is shown that the PB model demonstrates good agreement with the experimental measurements in the above two systems. It is expected that this study will provide guidance in the interpretation of experimental measurements and observations as well as in the design of $PbTiO_3$ films with specific thicknesses and domain stabilities.

Author's personal copy

Acknowledgements

The authors are grateful for financial support from the Department of Energy Basic Sciences under Grant No. DOE DE-FG02-07ER46417. The computer simulations were carried out on the LION clusters at The Pennsylvania State University, in part supported by instrumentation (cyberstar Linux cluster) funded by the National Science Foundation through Grant OCI-0821527 and in part by the Materials Simulation Center and the Graduate Education and Research Services at The Pennsylvania State University.

References

[1] Schlom DG, Chen LQ, Eom CB, Rabe KM, Streiffer SK, Triscone JM. Annu Rev Mater Res 2007;37:589.
[2] Setter N, Damjanovic D, Eng L, Fox G, Gevorgian S, Hong S, et al. J Appl Phys 2006;100:051606.
[3] Haeni JH, Irvin P, Chang W, Uecker R, Reiche P, Li YL, et al. Nat Lond 2004;430:758.
[4] Choi KJ, Biegalski M, Li YL, Sharan A, Schubert J, Uecker R, et al. Science 2004;306:1005.
[5] Spaldin NA. Science 2004;304:1606.
[6] Shaw TM, Trolier-McKinstry S, McIntyre PC. Annu Rev Mater Sci 2000;30:263.
[7] Fong DD, Stephenson GB, Streiffer SK, Eastman JA, Auciello O, Fuoss PH, et al. Science 2004;304:1650.
[8] Li S, Eastman J, Li Z, Vetrone JM, Foster CM, et al. Jpn J Appl Phys 1997;36:5169.
[9] Tybell T, Ahn CH, Triscone J-M. Appl Phys Lett 1999;75:856.
[10] Junquera J, Ghosez P. Nat Lond 2003;422:506.
[11] Lichtensteiger C, Triscone JM, Junquera J, Ghosez P. Phys Rev Lett 2005;94:047603.
[12] Pompe W, Gong X, Suo Z, Speck JS. J Appl Phys 1993;74:6012.
[13] Nagarajan V, Junquera J, He JQ, Jia CL, Waser R, Lee K, et al. J Appl Phys 2006;100:051609.
[14] Pertsev NA, Zembilgotov AG, Tagantsev AK. Phys Rev Lett 1998;80:1988.
[15] Pertsev NA, Koukhar VG. Phys Rev Lett 2000;84:3722.
[16] Bungaro C, Rabe KM. Phys Rev B 2004;69:184101.
[17] Diéguez O, Tinte S, Antons A, Bungaro C, Neaton JB, Rabe KM, et al. Phys Rev B 2004;69:212101.
[18] Li YL, Hu SY, Liu ZK, Chen LQ. Appl Phys Lett 2001;78:3878.
[19] Li YL, Hu SY, Liu ZK, Chen LQ. Acta Mater 2002;50:395.
[20] Alpay SP, Roytburd AL. J Appl Phys 1998;83:4714.
[21] Slutsker J, Artemev A, Roytburd AL. Acta Mater 2004;52:1731.
[22] Qiu QY, Nagarajan V, Alpay SP. Phys Rev B 2008;78:064117.
[23] Qiu QY, Mahjoub R, Alpay SP, Nagarajan V. Acta Mater 2010;58:823.
[24] Speck S, Pompe W. J Appl Phys 1994;76:466.
[25] Matthews JW, Blakeslee AE. J Cryst Growth 1974;27:118.
[26] People R, Bean JC. Appl Phys Lett 1985;47:322.
[27] People R, Bean JC. Appl Phys Lett 1986;49:229.
[28] Palova L, Chandra P, Rabe KM. Phys Rev B 2007;76:014112.
[29] Balzar D, Ramakrishnan PA, Hermann AM. Phys Rev B 2004;70:092103.
[30] Marée PMJ, Barbour JC, Van der Veen JF, Kavanagh KL, Bulle-Lieuwma CWT, Viegers MPA. J Appl Phys 1987;62:4413.
[31] Fox BA, Jesser WA. J Appl Phys 1990;68:2801.
[32] Price GL. Phys Rev Lett 1991;66:469.
[33] Venkatesan S, Vlooswijk A, Kooi BJ, Morelli A, Palasantzas G, De Hosson JTM, et al. Phys Rev B 2008;78:104112.
[34] Kwak BS, Erbil A, Budai JD, Chrisholm MF, Boatner LA, Wilkens BJ. Phys Rev B 1994;49:14865.
[35] Wemple SH. Phys Rev 1965;137:A1575.
[36] Devonshire AF. Philos Mag Suppl 1954;3:85.
[37] Haun MJ, Furman E, Jang SJ, Mckinstry HA, Cross LE. J Appl Phys 1987;62:3331.
[38] Li YL, Chen LQ, Asayama G, Schlom DG, Zurbuchen MA, Streiffer SK. J Appl Phys 2004;95:6332.
[39] Kwak BS, Erbil A, Wilkens BJ, Budai JD, Chisholm MF, Boatner LA. Phys Rev Lett 1992;68:3733.
[40] Hsu WY, Raj R. Appl Phys Lett 1995;67:792.